Femtosecond real-time probing of reactions. XIV. Rydberg states of methyl iodide

HUA GUO[1] AND AHMED H. ZEWAIL

Arthur Amos Noyes Laboratory of Chemical Physics,[2] California Institute of Technology, Pasadena, CA 91125, U.S.A.

Received October 7, 1993

This paper is dedicated to Professor John C. Polanyi on the occasion of his 65th birthday

HUA GUO and AHMED H. ZEWAIL. Can. J. Chem. **72**, 947 (1994).

The elementary reaction dynamics of methyl iodide in two Rydberg states leading to an iodine and a methyl radical occur on the femtosecond time scale (M.H. Janssen, M. Dantus, H. Guo, and A.H. Zewail. Chem. Phys. Lett. **214**, 281 (1993)). In this article, we consider the dynamics of this elementary process which involves both the Rydberg and valence states. Direct comparisons are made between theory and experiment with special focus on the following observations: large isotope effects, mode dependence of the predissociation rates, and coherence effects. The quantal molecular dynamics in two-dimensions show that the initial wave packet motion occurs along a vibrational mode involving the light atoms accompanied by transitions from the Rydberg state to the repulsive state; subsequent dynamics on the dissociative state lead to the C—I bond cleavage. The theoretical calculations also give the decay behavior of the Rydberg states with lifetimes in agreement with those observed in the femtosecond experiments. Moreover, the large isotope effect in observed predissociation rates of CH_3I and CD_3I has been successfully reproduced by the same model. The two-dimensional dynamics underscore the shortcomings of a one-dimensional picture in which the C—I serves as the sole reaction coordinate. The model presented here offers a viable mechanism for the dynamics of these Rydberg states.

HUA GUO et AHMED H. ZEWAIL. Can. J. Chem. **72**, 947 (1994).

La dynamique de la réaction élémentaire de l'iodure de méthyle dans les deux états de Rydberg conduit à des radicaux iode et méthyle dans un temps de l'ordre de la femtoseconde (M.H. Janssen, M. Dantus, H. Guo et A.H. Zewail. Chem. Phys. Lett. **214**, 281 (1993)). Nous considérons dans cet article la dynamique de ce processus élémentaire qui implique à la fois les états de Rydberg et la valence. On a comparé directement la théorie et l'expérimentation en mettant l'accent spécialement sur les observations suivantes: un large effet isotopique, l'influence du mode sur la vitesse de prédissociation et les effets de cohérence. La dynamique moléculaire quantique en deux dimensions montre que le mouvement du paquet d'ondes initial se produit le long d'un mode vibrationnel impliquant les atomes légers accompagné des transitions à partir des états de Rydberg jusqu'à l'état de répulsion; les dynamiques subséquentes relatives à l'état de dissociation conduisent au clivage de la liaison C—I. Les calculs théoriques donnent également la dégradation des états de Rydberg avec des temps de vie correspondant à ceux observés dans les expériences de l'ordre de la femtoseconde. De plus, le même modèle a permis de reproduire avec succès, le large effet isotopique dans les vitesses de prédissociation observées du CH_3I et du CD_3I. La dynamique bi-dimensionnelle met en évidence les défauts d'une image monodimensionnelle dans laquelle la liaison C—I représente la seule coordonnée de la réaction. Les modèles présentés offrent un mécanisme viable pour la dynamique de ces états de Rydberg.

[Traduit par la rédaction]

1. Introduction

The elementary processes of dissociation in methyl iodide (CH_3I) and its deuterated isotope (CD_3I) have been the subject of intensive investigations, both experimentally and theoretically. Most studies, guided by the theoretical analysis of Mulliken and Teller (1), were concerned (2–32) with the first absorption band which is structureless from 350 to 190 nm with a peak at 260 nm (2). This so-called A band arises from an electronic transition from a non-bonding $5p\pi$ orbital to a C—I antibonding σ orbital ($n \rightarrow \sigma^*$). Due to the strong spin–orbit coupling of iodine, five electronic states are formed in this manifold. They are, according to Mulliken (1), $^1Q_1(\Pi)$, $^3Q_2(\Delta)$, $^3Q_1(^3\Pi)$, $^3Q_{0+}(^3\Sigma^+)$, and $^3Q_{0-}(^3\Sigma^-)$. Since all the five states are repulsive in the C—I coordinate, the absorption of photon results in prompt fragmentation of methyl iodide. Both real-time measurements (3) and photofragment anisotropy analyses (4) have shown that the dissociation time in the A band is of the order of 100 fs.

The dissociation products from the *A* state excitation include both the ground and excited spin–orbit states of the iodine atom and methyl radical in its ground electronic state (5–8). the ro-vibrational state distributions of the methyl radical have been determined using various experimental techniques. It has been shown that the majority of dissociation energy is channeled into the translational recoil of the fragments and a relatively small portion of the excess energy is disposed into the umbrella bending (ν_5) of the methyl fragment (9–16) and its rotation about the axis perpendicular to the C_3 axis (14, 17, 18). Resonance Raman studies of the dissociation process have demonstrated the involvement of various vibrational modes in the process of fragmentation (19–23).

The dissociation from the A band is reasonably well understood theoretically. *Ab initio* potential energy surfaces have been calculated for the A band states (24, 25). It has been suggested (26) that the dissociation dynamics of CH_3I can be modeled by a collinear triatomic model where the umbrella bend of the CH_3 moiety can be approximated by a stretch between C and H_3. This approximation seems to be adequate for simulating most experimentally observed data. Both quantal (26–29) and classical (30–32) dynamical studies based on this model have been reported and the agreement between the two is generally very promising. Very recently, one of us (33) has reported a three-dimensional quantal study of the dissociation of methyl iodide in the A band, using the *ab initio* potential energy surfaces calculated by Morokuma and co-workers (25). Both the rotational and vibrational distributions of the methyl fragments as well as the I^* yield are in good agreement with latest experimental data (14–18).

[1]On leave from Department of Chemistry, University of Toledo, Toledo, OH 43606, U.S.A.

[2]Contribution No. 8869.

In this work, we focus on the dissociation dynamics of several Rydberg states which have higher absorption bands. Despite the vast literature on the A band dissociation, there is little known about the Rydberg states. The Rydberg character of the series can be largely attributed to transitions from a $5p$ orbital to a higher atomic Rydberg orbital, such as $6s$ or $6p$, of the iodine atom (1). The Rydberg series starts at 200 and 184 nm with two distinct bands, known as the B and C bands (34, 35). Both absorption bands are the result of an excitation of a non-bonding $5p\pi$ electron to the first Rydberg orbital ($6s$) of the iodine atom. The strong spin–orbit coupling at the iodine atom causes the splitting of the ion core into $^2E_{1/2}$ and $^2E_{3/2}$ in C_{3v} or $^2\Pi_{1/2}$ or $^2\Pi_{3/2}$ in $C_{\infty v}$, and interactions between the core and Rydberg electron yield five electronic states in two groups separated by approximately 5000 cm^{-1} (1). The B band is derived from the two lower states with a $^2E_{3/2}$ ion core, and the other three states (two are near degenerate) with a $^2E_{1/2}$ ion core are responsible for the C band. Traditionally (36), these states are named as the [1], [2], [3], and [4] states of the $6s$ transition. Similar arguments apply to higher Rydberg absorption bands which are originated from excitations of a non-bonding $5p\pi$ electron to higher Rydberg orbitals of iodine, such as $6p$ and $7s$, etc. In general, each Rydberg manifold splits into two bands characterized by the $^2E_{3/2}$ and $^2E_{1/2}$ ion cores with two distinguishable states for each band. Similar rules apply to the CH_3I^+ ion which can be loosely considered as a Rydberg state with the Rydberg electron infinitely far from the ion core.

The absorption spectra of these Rydberg states have been recorded by several groups (36–44). Felps et al. (36) have measured the one-photon absorption spectra of the B and C bands and extracted frequencies of various modes from the spectra. Resonance enhanced multiphoton ionization (REMPI) and other methods have also been employed to obtain the absorption spectra of methyl iodide (37–43). In particular, Vaida et al. (39–41) have examined the absorption of CH_3I and its clusters with a special interest on the effect of the cluster induced potential shift on the predissociation (42).

The higher $5p\pi \rightarrow 6p$ transitions near 170 and 150 nm have been investigated by Gedanken et al. (44) using (2 + 1) REMPI and by Tsukiyama et al. (45) using fluorescence spectroscopy. Similar to the $5p\pi \rightarrow 6s$ transitions, two bands with a separation of 5000 cm^{-1} were observed. The assignment of the vibronic transitions in this region was made by Gedanken et al. (44). In a recent study by Dobber et al. (46), who used both picosecond and nanosecond REMPI spectroscopy coupled with photoelectron spectroscopy (PES), a comprehensive analysis has led to the reassignment of the $6p$ and $7s$ Rydberg manifolds. These authors (46) were able to identify the feature near 311 nm (155.5 nm in two photons) as the band origin of the $5p\pi \rightarrow 7s$ transition, instead of the ν_6 overtone of the $5p\pi \rightarrow 6p$ transition assigned previously (44).

From the above studies, it has been realized that the transitions from the ground state to various Rydberg states are rather vertical. The vibrational progressions are short and the band origins usually represent the strongest transitions. This is because the Rydberg excitation (including the ionization) from a non-bonding orbital ($5p\pi$) does not significantly alter the molecular geometry of the molecule (or ion). As a result, the vibrational frequencies as well as the equilibrium geometry of various Rydberg states are very similar to those of the ground electronic state (37, 38, 44, 46, 47). All the Rydberg features of methyl iodide are significantly broadened. The broadening is associated with the predissociation of these Rydberg states since the line width is less than the vibrational spacing.

The rates of predissociation have been deduced for the first two Rydberg states (the B and C bands) using various techniques. An early photofragment anisotropy analysis at 193 nm (48) estimated that the lifetime of CH_3I is approximately 150 fs. Ziegler and co-workers (49) have deduced the lifetimes of the B (50–52) and C (53) Rydberg states by monitoring the depolarization ratio of Raman scattering, in which the average rotation of the molecule is utilized as an effective clock. The lifetimes of the B and/or C Rydberg states obtained by these authors range from 10^2 to 10^3 fs and the lifetime data exhibit strong isotopic and mode selectivities (51). For instance, it was found (51) that the lifetime of CD_3I is a factor of two longer than that of CH_3I. Recently, information on lifetimes was also obtained from the direct measurement of the absorption profile, as reported by Syage (43).

Large discrepancies were found among reported lifetimes in the *B* and *C* states. For example, Sapers and Donaldson (38) reported a much faster predissociation rate for the first ν_3 (C—I stretch) overtone in the B band than the band origin. This conclusion was advanced to explain the observation that the ν_3 feature is present in the dimer but disappears in the monomer. Wang and Ziegler (51), from the Raman analysis of the same system, concluded that the decay rate of the first ν_3 overtone is much slower than both the band origin and the second ν_3 overtone. A simple Franck–Condon model was proposed by these authors to rationalize the experimental findings (51). Both results (38, 51), although in opposite directions, pointed to strong mode specificity in the predissociation of methyl iodide Rydberg states. The latest study on the same system (43), however, reported very weak mode-specific predissociation rates for the band origin and the first ν_3 overtone.

Theoretically, the predissociation of Rydberg states of methyl iodide have been studied by several groups. Donaldson et al. (54) reported classical trajectory studies on the predissociation in the B band. These authors utilized empirical potential energy surfaces to investigate the dissociation dynamics and the influence of the cluster on the curve crossing process. Wang and Ziegler (51) proposed a simple Franck–Condon model to interpret their findings of slow predissociation rate of the ν_3 overtone (see above). These studies have not addressed the femtosecond quantum dynamics and, in particular, the large isotope and coherence effects in the predissociation.

Real-time studies of the Rydberg state dynamics of methyl iodide in a molecular beam have been reported using femtosecond transition-state spectroscopy (FTS) (55). In these studies (56, 57), a molecular beam of methyl iodide was excited by a femtosecond (fs) pulse near the $6p$–$7s$ manifold (by two photons) and subsequently ionized by another fs pulse. The resulting parent (CH_3I^+) or fragment ions (CH_3^+ and I^+) were detected in a time-of-flight mass spectrometer. The ionization pulse was delayed from the excitation pulse so that the dynamics of the Rydberg state could be probed with femtosecond resolution. The transients show that the decay of the Rydberg states is on the femtosecond time scale. For example, the $6p[4]$ band origin was found to decay with a lifetime of 178 fs (56, 57). The experiment also shows that there is a strong isotope effect; the lifetime of CD_3I is at least two times longer than that of the CH_3I. Mode specificity in predissociation dynamics was found to be weak in the energy range studied, as the first ν_3 overtone decays only slightly faster than the band origin (57).

To examine the predissociation dynamics on the femtosecond time scale, we have initiated quantum mechanical studies of these Rydberg states in one and two dimensions (57, 58). Classical mechanics and one-dimensional models are not adequate for reasons discussed below. Our preliminary results in two dimensions show that the large isotope effect in the predissociation of the Rydberg states can be attributed to the involvement of the C—H_3 stretch in the dissociation pathway. The experimentally measured transients for the band origin of the $5p\pi \rightarrow 6p[4]$ transitions were nicely reproduced for both CH_3I and its deuterated isotope CD_3I.

In this contribution, we provide a full account of this two-dimensional quantum mechanical model, focusing on the acute isotope effect in dynamics, mode selectivity, and coherence effects. We discuss the nature of the Rydberg-valence state coupling and the non-adiabatic transition dynamics along the reaction coordinate. This paper is organized as follows. In Section II, a brief description of the experimental results is given. In Section III, we discuss the rationale for the newly developed empirical potential energy surfaces for both the Rydberg and dissociative states, and the time-dependent quantum mechanical method used in our calculations. In Section IV, the results from the calculation are presented. The implication of the results and general features of the Rydberg dynamics are discussed in the Section IV.

II. Experimental

As mentioned earlier and detailed elsewhere (56, 57), the Rydberg levels of CH_3I and CD_3I were selectively excited via a femtosecond coherent two-photon absorption. The dynamics of the Rydberg states were then probed by a temporally delayed pulse which ionizes the parent molecule to its ions. This femtosecond pump–probe scheme (with mass resolution) is different from previous REMPI studies using nanosecond or picosecond lasers (44–46). It is well known that the A band states, which serve as the intermediate states for the two-photon excitation ladder, are strongly dissociative with a lifetime of ~100 fs (3–5). Therefore, unless the pulse duration is comparable with or shorter than the dissociation time of the A states, the two-photon transition will be overwhelmed by the one-photon dissociation in lower A band. This phenomenon is clearly illustrated in the nanosecond REMPI studies of methyl iodide (44, 46) where the spectra are contaminated by sharp transitions of the iodine atoms produced from the A band fragmentation. Such a behavior is avoided in the REMPI using femtosecond pulses.

Femtosecond transients were taken at several pump wavelengths (57). Here, we concentrate on three of them, i.e., transitions to the band origin and first ν_3 overtone of the $6p[4]^2E_{1/2}$ Rydberg state and to the band origin of the $7s[1]^2E_{3/2}$ Rydberg state. The three transitions have two-photon excitation energies of 63 493 cm^{-1} (λ_{pump} = 315 nm), 63 958 cm^{-1} (λ_{pump} = 312.5 nm) and 64 230 cm^{-1} (λ_{pump} = 311.5 nm), respectively. The ionization laser has a wavelength of 618 nm. Figure 1 presents the absorption spectrum of methyl iodide (CD_3I) in this spectral region with the assignments by Dobber et al. (46). Two types of pump pulses with different bandwidths were used in the experiment (57). Their excitation bandwidths are 1.5 and 3.5 nm at ~320 nm, respectively. With the broad bandwidth pump pulse, it is possible to excite two vibronic bands coherently, which may lead to interesting dynamics (57), as discussed below.

The transients measured using narrow bandwidth pump pulses can be fitted to single exponential functions, from which the lifetime of the Rydberg state can be obtained. Table 1 lists the lifetimes of individual Rydberg states for both CH_3I and CD_3I. It is clear that no mode selectivity in the lifetime of the $6p[4]^2E_{1/2}$ state is weak in the energy range studied. The lifetime of the band origin (178 fs) is only slightly longer than that of the first ν_3 overtone (141 fs) of $6p[4]^2E_{1/2}$ Rydberg state. The FTS measurements have also been made for the deuterated methyl iodide. It was found that the decay time of CD_3I is generally a factor of two or more slower than that of CH_3I, as shown in Fig. 2a.

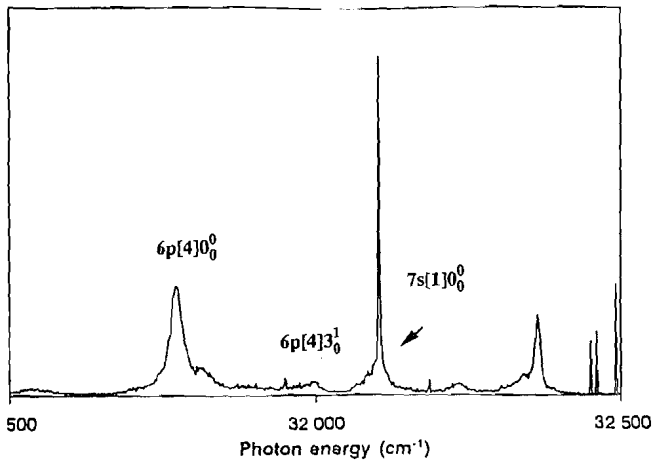

FIG. 1. Experimental Rydberg state absorption spectrum of the CD_3I near 64 000 cm^{-1} (adopted from Dobber et al. (46)). Note that the sharp feature near 32 100 cm^{-1} is due to an atomic iodine transition and is irrelevant to the molecular Rydberg absorption.

TABLE 1. Experimental lifetimes of Rydberg levels

λ^a (nm)	Level[b]	Lifetimes (fs) CH_3I	Lifetimes (fs) CD_3I
315.0/b	$6p[4]0_0^0$	178	333
314.7/n	$6p[4]0_0^0$	183	—
312.7/n	$6p[4]3_0^1$	141	—
312.0/b	$\{6p[4]3_0^1 + 7s[1]0_0^0\}$	141	414
311.3/n	$7s[1]0_0^0$	115	—

[a]Letters n and b denote narrow and broad bandwidths of the pump pulses, respectively.

[b]The vibrational modes of CH_3I are defined as follows (34): the symmetric C—H_3 stretch (ν_1), the umbrella C—H_3 bend (ν_2), the C—I stretch (ν_3), the antisymmetric C—H_3 stretch (ν_4), the CH_3 deformation (ν_5), and the I—C—H_3 bend (ν_6).

The broadening of the pump pulse bandwidth does not significantly alter the lifetime of the band origin of the $6p[4]^2E_{1/2}$ Rydberg state (57). When the broad bandwidth pulse was tuned to 311 nm, however, the experimental transient could not be fitted to a single exponential (see Fig. 2b). It seems that the transient contains a double peak structure or a damped oscillatory structure with a frequency of 7×10^{12} Hz (Δt = 140 fs) at the initial stage of the dynamics. A similar effect has been found for the same Rydberg feature of the deuterated methyl iodide. It should be noted that the broad bandwidth pulse covers coherently both the first ν_3 overtone of the $6p[4]^2E_{1/2}$ state and the band origin of the $7s[1]^2E_{3/2}$ state, which have an energy separation of 240 cm^{-1} (see Fig. 1). This point will be discussed in more detail later when we discuss the coherence effect.

III. Theoretical model

A one-dimensional model was recently proposed to simulate the observed femtosecond dynamics of methyl iodide Rydberg predissociation (58). In this model, only the C—I coordinate was considered and the predissociation dynamics were modeled by non-adiabatic transitions from the Rydberg state to a dissociative state using a quantum mechanical method. The results indeed showed a slightly slower predissociation rate for the deuterated methyl iodide than that of CH_3I, but the cal-

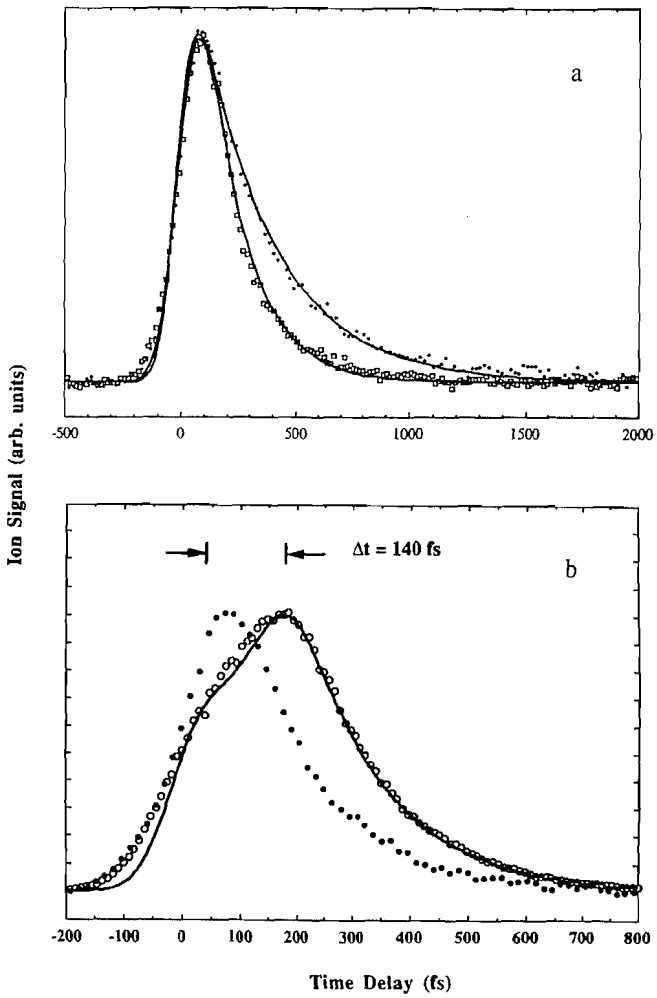

FIG. 2. Femtosecond transients obtained (*a*) for 315 nm two photon excitation for CH_3I (open square) and CD_3I (filled circles) (adopted from Dantus et al. (56)), and (*b*) for 312 nm two-photon excitation of CH_3I (adopted from Janssen et al. (57)). A transient has been superimposed (filled circles) in (*b*) to highlight the large difference in shape occurring when the $6p[4]\ 3_0^1$ and $7s[1]\ 0_0^0$ modes are overlapped by the excitation-laser bandwidth (see text).

culated isotope effect was significantly smaller than the ratio found experimentally. The implication is that the C—I mode may not be the major contributor of the initial predissociation reaction pathway. This can be readily understood in terms of the ratio of the reduced masses of the deuterated and hydrogenated methyl iodide species, which is 1.18. The significant isotope effect indicates the involvement of modes other than the dissociating C—I coordinate. One possibility is that the molecule dissociates through a barrier involving light atom (H or D) tunneling. An overall slowdown of the deuterated predissociation dynamics is hence expected because the tunneling probability decreases exponentially with mass.

We in this work propose a new predissociation mechanism for the CH_3I Rydberg states by including another nuclear mode. Our choice of the additional mode is the ν_1 vibration, i.e., the symmetries C—H_3 stretch (58). The reduced mass of the C—H_3 mode is 1.67 times smaller than that of C—D_3, which may result in a large isotope effect. It should be pointed out that the choice of the ν_1 mode is to some extent arbitrary because the dissociation may well involve one or many other modes that have large mass differences, such as the antisymmetric C—H_3 stretch (ν_4) or umbrella bend (ν_5) modes, etc. Our purpose here is to illustrate the importance of the multidimensional effect on the predissociation dynamics. There is some evidence indicating the involvement of the ν_1 mode in the predissociation. For example, resonance Raman measurements (50–53) on lower B and C Rydberg states concluded that the excitation in the C—H_3 symmetric stretch leads to much faster decay rates for both CH_3I and CD_3I. Photofragmentation experiments (48, 60) also found significant excitation of the fragment C—H vibration and even cleavage of a C—H bond during the dissociation for photon wavelengths shorter than 170 nm. In the next subsection we will develop empirical potential energy surfaces for both the Rydberg and dissociative states for the CH_3I system based on these arguments. The dynamical calculations on these potential energy surfaces will be detailed in the second subsection.

A. Potential energy surfaces

The existing *ab initio* calculations of methyl iodide potential energy surfaces (24, 25) are mainly concerned with the low-lying A manifold and the ground electronic state. Information on the Rydberg potential energy surfaces is mostly from spectroscopic data. It is well known from absorption studies that the potential energy surfaces of the Rydberg states are very similar to that of the ground state. The normal frequencies of the Rydberg states are found to be comparable with those on the ground state (36, 44, 46). The similarities between the ground and Rydberg states of methyl iodide indicate that the Rydberg transitions have little impact on the molecular parameters of the CH_3I ion core. Such a phenomenon is due to the fact that the Rydberg transition is from a non-bonding orbital ($5p\pi$) to an atomic orbital ($6s$, $6p$, or $7s$ etc.).

Throughout this work, we will limit ourselves to a two-dimensional model which involves both the C—I (ν_3) and C—H_3 (ν_1) vibrational modes. Empirical potential energy surfaces are developed to possess certain important features which will result in an accurate reproduction of experimental findings. For instance, the intersection between the Rydberg state and the repulsive state (i.e. the seam) is arranged in such a way that the isotope effect in the predissociation can be correctly represented. We have manipulated the potentials so that the seam is perpendicular to the C—H_3 coordinate in the Franck–Condon region, rather than to the C—I dissociation mode as assumed in the one-dimensional calculations (58). Thus, the dissociation is more likely to proceed along the C—H_3 coordinate at the beginning of the dissociation. Subsequent dissociation will then lead to the C—I bond cleavage. The resulting reaction pathway therefore involves both the C—I and C—H_3 modes and the dissociation should show a much larger isotope effect due to the significantly larger differences in both the reduced mass and zero point energy during the initial pr dissociation dynamics. The nature of similar reaction path been addressed recently in the work of Nikitin and co-wor (59).

For the sake of simplicity, the potential energy surfa the ground state, the Rydberg state and the repulsive s all written as sums of two one-dimensional potentials. aration of modes in the model potential energy surfa not affect the dynamics because the potentials ar relative to each other. The ground electronic st energy surface consists of a Morse function in ordinate (R) and a quadratic potential for C— (*r*):

TABLE 2. Parameters of potential energy surfaces (atomic units[a])

Parameter	Value	Parameter	Value	Parameter	Value	Parameter	Value	Parameter	Value
D_1	0.08741	R_{01}	4.1688	r_{01}	2.0503	α_1	0.9150	ϵ_1	-0.2893
D_2	0.07153	R_{02}	4.2576	r_{02}	2.0503	α_2	0.8295	ϵ_2	0.0000
D_3	18.3673	R_{03}	0.0	r_{03}	2.5503	α_3	1.30	ϵ_3	-0.1044
						α_{23}	0.50		
D_{23}	0.028					$k_{01} = k_{02} = k_{03} = 0.8066$			

[a] 1.0 Å = 1.8898 au (Bohr), 1.0 eV = 0.03675 au (Hartree).

$$[1] \qquad V_1 = D_1\{1 - \exp[-\alpha_1(R - R_{01})]\}^2 + \tfrac{1}{2}k_1(r - r_{01})^2 + \epsilon_1$$

Similar form of potential energy function is given for the Rydberg state:

$$[2] \qquad V_2 = D_2\{1 - \exp[-\alpha_2(R - R_{02})]\}^2 + \tfrac{1}{2}k_2(r - r_{02})^2 + \epsilon_2$$

The Morse potential of the Rydberg state is slightly different from that of the ground state, reflecting changes in molecular parameters. The C—H_3 potential, on other hand, is chosen to be identical to that of the ground state. The selection of the potential parameters is consistent with the absorption spectrum of Rydberg states of methyl iodide (44, 46), as shown below.

There is little known about the nature of the dissociative state which interacts with the Rydberg state. This dissociative state is "optically dark" and information from *ab initio* calculations is sketchy. There are some suggestions that it may be one of the five A band states (57). For the zeroth order, we assume that it is repulsive in the C—I coordinate and bound in the C—H_3 coordinate. An exponential function is used for the C—I mode and a harmonic oscillator potential is adopted for the C—H_3 mode:

$$[3] \qquad V_3 = D_3 \exp[-\alpha_3(R - R_{03})] + \tfrac{1}{2}k_3(r - r_{03})^2 + \epsilon_3$$

The C—H_3 potential in eq. [3] has the same force constant as the ground state, but is shifted from the ground state C—H_3 equilibrium geometry. Such a shift enables the dissociative state to form an intersection with the Rydberg state in the direction perpendicular to the C—H_3 coordinate. As discussed earlier, the location of the intersection is vital in simulating the experimentally observed isotope effect. As shown in the one-dimensional calculations (58), the alternative would be an intersection perpendicular to the C—I coordinate, which would only produce a limited isotope effect. It should be pointed out that this potential energy surface is not expected to give the correct asymptotic properties of the CH_3 fragment. However, this deficiency would have little effect on the Rydberg dynamics which occurs at relatively small C—I distances.

The parameters of all the three potential energy surfaces are given in Table 2. The potential energy surfaces of both the bound Rydberg and dissociative states are plotted in Fig. 3. The intersection between the two potential energy surfaces is nearly perpendicular to the C—H_3 coordinate, as shown in the figure. Three dimensional view of the lower adiabatic potential energy surface is also given in Fig. 3*b*.

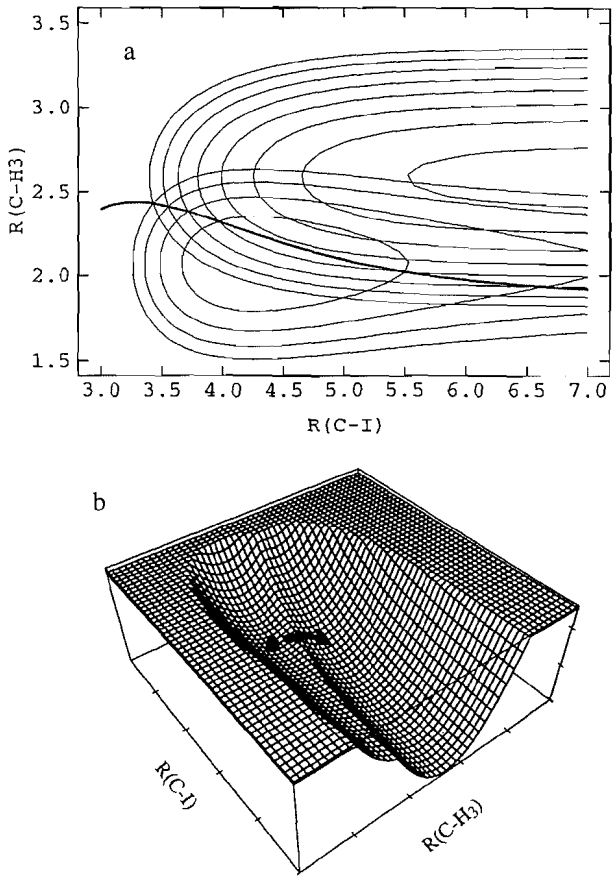

FIG. 3. (*a*) Diabatic potential energy surfaces of the $6p[4]^2E_{1/2}$ Rydberg state and the dissociative state. The intersection (seam) of the two potential energy surfaces is also given with a heavy black line. The energy interval of the contours is 0.03 au. (*b*) Three dimensional view of the lower adiabatic potential energy surface. The C—I and C—H_3 coordinates are from (3.0, 1.0) to (6.0, 4.0) au. The Franck–Condon region is showed by the black spot and the minimal energy path is indicated by the arrow.

B. Time-dependent quantum mechanical theory

Theoretical studies of the femtosecond dynamics have been reported by many groups (see, e.g., refs. 61–71). In this work, we employ a time-dependent quantum mechanical description of such a process. The nuclear Hamiltonian of the methyl iodide Rydberg system including the light–molecular interaction is given in a diabatic representation (58):

$$[4] \qquad \mathbf{H} = \begin{bmatrix} \mathbf{h}_{11} & \mathbf{h}_{12} & \mathbf{0} & \mathbf{0} \\ \mathbf{h}_{12}^* & \mathbf{h}_{22} & \mathbf{h}_{23} & \mathbf{h}_{24} \\ \mathbf{0} & \mathbf{h}_{23}^* & \mathbf{h}_{33} & \mathbf{0} \\ \mathbf{0} & \mathbf{h}_{24}^* & \mathbf{0} & \mathbf{h}_{44} \end{bmatrix}$$

where the asterisk denotes complex conjugate. There are at least four states involved in the pump-probe experiment (57). An additional state is needed when the electronic coherence effect is studied. The ground electronic state (state 1) is coupled radiatively ($\mathbf{h}_{12}$) with the Rydberg state (state 2). The non-adiabatic or radiationless interaction ($\mathbf{h}_{23}$) between the Rydberg state and the dissociative state (state 3) is responsible for the predissociation. The dynamics on the Rydberg state are probed by a delayed pulse ($\mathbf{h}_{24}$) which promotes the molecule to the ion state (state 4). The diagonal terms in the Hamiltonian matrix consist of the kinetic and potential energy operators:

$$[5] \qquad \mathbf{h}_{ii} = \frac{\mathbf{p}_R^2}{2\mu_R} + \frac{\mathbf{p}_r^2}{2\mu_r} + V_i(R, r)$$

where V_i are the diabatic potential energy surfaces defined in the last subsection; μ_R and μ_r are appropriate reduced masses for the two coordinates. The overall rotation of the parent molecule is not included in our model since the dissociation time of the Rydberg states is much shorter than the rotational period. Other degrees of freedom of methyl iodide are also assumed to be separable from the reaction coordinates and not considered here. The off-diagonal matrix terms representing the non-adiabatic coupling are given by the coupling potential:

$$[6] \qquad \mathbf{h}_{23} = V_{23} = D_{23} \exp[-\alpha_{23}R]$$

The potential parameters for the non-adiabatic coupling are given in Table 2.

Within the dipole and classical electromagnetic field approximations (63, 67, 72), the light-molecular interactions are given by

$$[7] \qquad \begin{aligned} \mathbf{h}_{12} &= A_{12}(t) \exp(i\omega_{12}t) \\ \mathbf{h}_{24} &= A_{24}(t-\tau) \exp(i\omega_{24}t) \end{aligned}$$

where ω_{12} and ω_{24} are the photon frequencies of the pump and probe pulses, respectively. τ denotes the time delay between the pump and probe pulses. The pre-exponential factor $A(t)$ consists of the appropriate transition dipole moment and the temporal shape of the pulse. The transition dipole moments are assumed to be constants of the nuclear coordinates (Condon approximation) because of the lack of information on their coordinate dependence. The laser pulses are assumed to have a Gaussian functional form (63):

$$[8] \qquad A(t-t_0) = A_0 \exp[-\beta(t-t_0)^2/2]$$

Where β determines the temporal width of the pulse and t_0 determines the time of the pulse.

The overall dynamics of the pump-probe process can be obtained by solving the time-dependent Schrödinger equation (atomic units are used hereafter) (58, 63, 67)]:

$$[9] \qquad i\frac{\partial}{\partial t}\begin{bmatrix}\varphi_1\\ \varphi_2\\ \varphi_3\\ \varphi_4\end{bmatrix} = \begin{bmatrix}\mathbf{h}_{11} & \mathbf{h}_{12} & \mathbf{0} & \mathbf{0}\\ \mathbf{h}_{12}^* & \mathbf{h}_{22} & \mathbf{h}_{23} & \mathbf{h}_{24}\\ \mathbf{0} & \mathbf{h}_{23}^* & \mathbf{h}_{33} & \mathbf{0}\\ \mathbf{0} & \mathbf{h}_{24}^* & \mathbf{0} & \mathbf{h}_{44}\end{bmatrix}\begin{bmatrix}\varphi_1\\ \varphi_2\\ \varphi_3\\ \varphi_4\end{bmatrix}$$

where φ_i are the nuclear wavefunctions on individual electronic states. Initially, only the ground state is populated and wavefunctions on all other states are assumed to be zero. The highly oscillatory phase factor in the radiative coupling (i.e., $\exp(i\omega t)$) can be absorbed into the wavefunction. The effect of this operation is to raise the ground state potential by the amount ω_{12} and lower the ion state potential by ω_{24} (63). Therefore, the radiative coupling can be effectively regarded as a time-dependent non-adiabatic coupling. Such a treatment not only avoids oscillations introduced by the field, which may substantially increase the number of temporal steps in numerical integration, but also simplifies the Schrödinger equation dramatically.

It is instructive to rewrite the Schrödinger equation in the integral form. For the Rydberg state, for example, its temporal evolution can be described by:

$$[10] \qquad \begin{aligned} \varphi_2(t) &= -i\int_{-\infty}^{t} dt' e^{[-i\mathbf{h}_{22}(t-t')]}[\mathbf{h}_{12}\varphi_1(t') \\ &\quad + \mathbf{h}_{23}\varphi_3(t') + \mathbf{h}_{24}\varphi_4(t')] \\ &= -i\int_{-\infty}^{t} dt' e^{[-i\mathbf{h}_{22}(t-t')]}[A_{12}(t')\varphi_1(t') \\ &\quad + V_{23}\varphi_3(t') + A_{24}(t'-\tau)\varphi_4(t')] \end{aligned}$$

The population of the Rydberg state as initial $t \rightarrow -\infty$ is zero. The first term in the integrand represents the transfer of population from the ground state to the Rydberg state while the pump pulse is switched on. Population is subsequently lost to the dissociative state via the non-adiabatic coupling V_{23}. When the probe pulse is switched on at time τ, some population is transferred to the ion state, which is represented by the third term. If the laser field is considered to be weak, a perturbative approach can be adopted (65, 69, 72). Under such circumstances, the ground state can be, to the first order, approximated by a stationary state and the population transferred back from the Rydberg state is negligible.

The experimentally measured ion transient signal is considered to be proportional to the asymptotic population of the ion state at different delay times. In our calculations, however, we have imposed an approximation that the ionization photon is on resonance with the energy gap between the Rydberg state and the ion state. Therefore, the ion state population at various delay times (the transient) is directly proportional to the temporal population on the Rydberg state except for a numerical factor representing the pulse shape (69). Photo-induced ionization processes are often considered as a Franck–Condon event. Since the electron ejected by the photon may carry different kinetic energies, even with the same ionization photon wavelength, its treatment requires special care (73, 74). Limited test calculations with all four states have been carried out and the transients obtained are almost identical to the temporal population of the Rydberg state. Another approximation in our calculations is the treatment of the pump pulse. We have assumed that the Rydberg state is prepared by a single photon whereas two coherent photons were used in the experiment to reach the Rydberg state. This simplification should not significantly affect the calculated results, other than the usual change in the pulse width and coherence width with multiphoton processes.

The numerical solution of the time-dependent Schrödinger equation was carried out on a two-dimensional grid. The temporal propagation of the coupled differential equations was accompanied by using a short iterative Lanczos (SIL) method (75). In the SIL method, a N-dimensional Krylov subspace

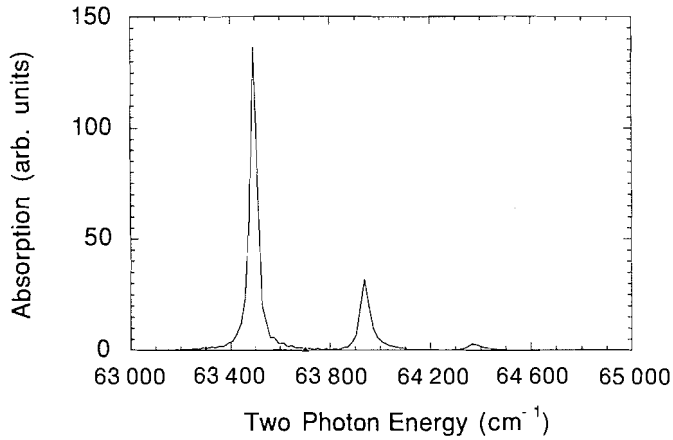

FIG. 4. Calculated absorption spectrum of the $6p[4]^2E_{1/2}$ Rydberg state of CH_3I using the model potential energy surfaces. The spectrum shows the strongest absorption is at the band origin and the ν_3 progression is weak.

spanned by $\mathbf{H}^N\Psi$ is constructed by the Lanczos recursion scheme. The propagator is then obtained from the eigenvalues and diagonalization matrix of effective Hamiltonian matrix in the subspace. It has been shown (75) to be efficient in dealing with both the time-dependent and time-independent Hamiltonians.

The evaluation of $\mathbf{H}\Psi$ was carried out in two steps. The action of the potential energy operator on the wavefunction can be readily obtained by multiplying the two at each grid point. The action of the kinetic energy operator was calculated in momentum space where the kinetic energy operator is diagonal. The wavefunction transformation between coordinate and momentum representations was carried out by using a fast Fourier transform (FFT) method (76). In order to avoid reflection on the edges of the grid, a damping scheme (77) was used at large R to eliminate the wave packet on the dissociative state. Since we are interested in the population decay on the bound Rydberg state, the damping at large C—I distances would not affect our simulation.

IV. Results and discussion

We used in the calculations a grid of 256 × 32 (R, r) points covering a rectangular region from (3.5, 1.0) to (7.5, 4.0) bohr. The temporal interval is 0.5 fs with an eight-dimensional Krylov space for the SIL propagator. The starting point of the propagation is −300 fs and the pump pulse is centered at 0 fs. The laser pulse was chosen to have an 80 fs temporal width (FWHM). The laser field strength was arbitrarily chosen to simulate a weak field scenario. Convergence tests have been conducted with respect to the sizes of both spatial and temporal grids.

A. Absorption, isotope effect, and mode selectivity

Figure 4 is the calculated absorption spectrum of the $6p[4]^2E_{1/2}$ Rydberg state of CH_3I. The spectrum was calculated from the Fourier transform of the autocorrelation function of the Rydberg state with a delta-function excitation pulse (78, 79). The energy resolution of the spectrum is approximately 17 cm^{-1} which corresponds to 2 ps of propagation. The calculated spectrum shows an intensive absorption near 63 500 cm^{-1} and two much weaker overtone excitations near 63 950 and 64 400 cm^{-1}, respectively, in good agreement with experiment (44, 46). Note that the equilibrium geometry

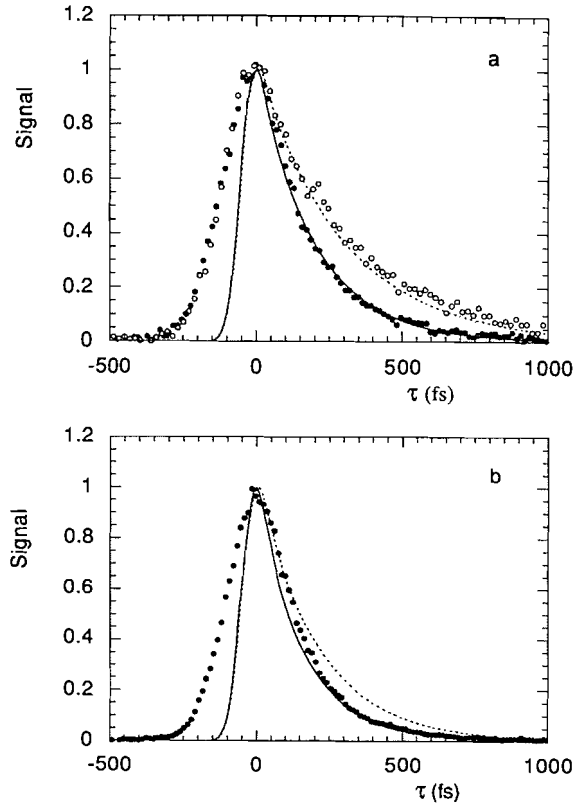

FIG. 5. Calculated femtosecond transient of the $6p[4]\ 0_0^0$ (*a*) and $6p[4]\ 3_0^1$ (*b*) Rydberg levels for both CH_3I (solid line) and CD_3I (dashed line). The experimental data (filled and open circles for CH_3I and CD_3I, respectively) are also given.

of the Rydberg state is shifted to a larger R relative to that of the ground state. The difference in the equilibrium geometry of the two states changes the Franck–Condon overlap and results in a weak progression in ν_3. No progression in the ν_1 mode is observed because the Rydberg state has the same C—H_3 potential as the ground state.

The transients of the first two vibrational levels of the $6p[4]^2E_{1/2}$ Rydberg state for both CH_3I and CD_3I are given in Fig. 5 together with corresponding experimental data. All the curves are normalized to unity and the zero time is arbitrarily chosen. The top panel is for the band origin of the $6p[4]^2E_{1/2}$ Rydberg state. The calculated decay curves not only fit the experimental transients, they also correctly reproduce the isotope effect observed in the experiment. The agreement between the two-dimensional model calculations and the experiments of CD_3I is particularly encouraging since our potential parameters were only adjusted to fit the CH_3I transient. Comparison with previous one-dimensional calculations (58) strongly supports the argument that the significant isotope effect is due to the involvement of tunneling of the light atoms during predissociation. The lower panel in Fig. 5 gives the transients of the first overtone of the ν_3 mode on the $6p[4]^2E_{1/2}$ Rydberg state. Experimental data are only available for the CH_3I species. The agreement again is rather satisfactory. The calculated results support the experimental observation that the ν_3 vibrational overtone predissociates slightly faster than the band origin.

Figure 6 shows a cut of the potential energy surfaces along the C—H_3 coordinate at the groundstate equilibrium C—I distance. The CH_3I low-lying vibrational levels of both the $6p[4]^2E_{1/2}$ and $7s[1]^2E_{3/2}$ Rydberg states also plotted in the

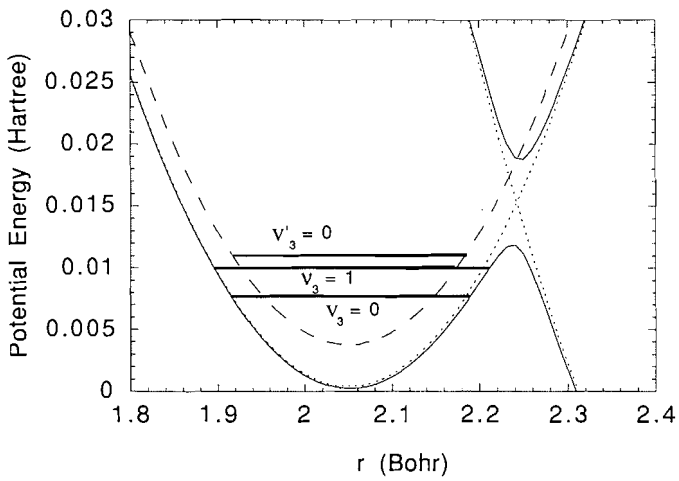

FIG. 6. Potential energy surface cuts in the C—H_3 coordinate at the ground state C—I equilibrium geometry. The dotted (the $6p[4]$ Rydberg and dissociative states) and dashed (the $7s[1]$ Rydberg state) lines are diabatic surfaces. The solid lines represent adiabatic surfaces formed between the $6p[4]$ Rydberg and dissociative states. Vibrational levels on the two Rydberg states are also given. Both the isotope effect and mode selectivity can be explained in the adiabatic picture (see text).

figure. The $6p[4]^2E_{1/2}$ Rydberg state intersects with the dissociative state at $r = 2.25$ au and they form two adiabatic surfaces due to the non-adiabatic coupling between the two states. It was found from our calculations that the coupling is significant so that the transition from the Rydberg state to the dissociative state is best described in the adiabatic representation. At the intersection, as shown in Fig. 6, the coupling is approximately 700 cm^{-1}. In order to reach the dissociation channel, the system has to tunnel through a barrier formed by the lower adiabatic surface. Since the deuterated methyl iodide has a much larger reduced mass in the r coordinate, it is more difficult to penetrate the barrier to dissociate. Furthermore, the CD_3I vibrational levels (not shown in the figure) are lower than their CH_3I counterparts because of the smaller zero point energy. The width of the barrier at these levels is thus relatively broader. Both factors contribute to the overall slowdown of the CD_3I predissociation.

The accelerated predissociation rate for the first ν_3 overtone can also be interpreted using the picture of Fig. 6. It can be clearly seen from the figure that the vibrational level for the first ν_3 overtone is much closer to the top of the barrier so that it is much easier to penetrate the barrier and dissociate. However, the increase in predissociation rate is small because the averaged kinetic energy is largely in the C—I direction.

B. Wave packet dynamics

As we indicated earlier in this paper, the model potential energy surfaces were developed in such a way that the predissociation proceeds initially along the C—H_3 coordinate and then leads to CH_3 and I. Indeed, the wave packet dynamics clearly show these characteristics of the potential energy surfaces. Snapshots of the decaying wave packet of CH_3I at 0, 10, 20, and 30 fs are plotted in Fig. 7. The lower *adiabatic* potential energy surface is also given in the background (heavy contours). In order to show the immediate propagation at short times, we used a delta function pulse for the excitation of the wave packet from the ground state. The wave packet shown in Fig. 7 is a sum of the wave packet modules on both the Rydberg and dissociative states. The wave packet is initially prepared on the Rydberg state, in the small well on the adiabatic surface (Fig. 7*a*).

In the first ten femtoseconds, the movement of the wave packet is mostly along the CH_3 coordinate (Fig. 7*b*) because the barrier to direct C—I bond cleavage is very high. The wave packet therefore chooses to make non-adiabatic transitions from the Rydberg state to the dissociative state along the C—H_3 coordinate. The part of the wave packet that escapes from the shallow well immediately experiences strong forces in both the C—H_3 and C—I directions. As a result, the wave packet starts to oscillate in the C—H_3 direction and accelerate down hill towards the dissociation of the C—I bond (Fig. 7*c* and *d*). These transitions are responsible for the decay of the Rydberg population shown in Fig. 5. It was found that there is no population recurrence in the Rydberg state and the decay can be readily fitted by an exponential function. The wave packet at large C—I distances is damped in the calculation since we are only interested in the dynamics of the parent CH_3I Rydberg state.

The oscillation in the C—H_3 coordinate will eventually lead to the excitation of the CH_3 fragment and such a motion is the analog of transition-state resonances (80). In the extreme cases, the excitation can result in the C—H bond cleavage. Although the asymptotic CH_3 internal energy is not of interest in this study, the strong oscillation in the C—H_3 mode is consistent with experimental observations of large vibrational excitation of the CH_3 fragment (48, 60).

C. Coherence effects

Finally, we would like to discuss the possible existence of coherence in the sufficiently broad bandwidth excitation near 312 nm (57). As shown in Fig. 2, the transient at 312 nm seems to have two peaks with a shift or an "oscillation period" of 140 fs. This frequency coincides with the energy difference between the $\nu_3 = 1$ vibrational level on the $6p[4]^2E_{1/2}$ Rydberg state and the $\nu_3 = 0$ level on the $7s[1]^2E_{3/2}$ Rydberg state. Since both vibrational levels could be coherently excited by a single pulse, there is a possibility that they may retain the coherence for some time provided that these two states are properly coupled. In this section, we will attempt to model coherence effects using wave packet dynamics.

The key in preparing a wave packet is to coherently excite more than one quantum state. In other words, these quantum states have to be excited by photons with the same phase. This was not possible experimentally until the introduction of the femtosecond lasers since only on this time scale a coherent nuclear wave packet could be formed at a given nuclear geometry (55). On a given potential, coherence can be manifested in a number of ways. For example, it has been shown in the case of I_2 (81) that a coherent wave packet can be prepared on an excited state by a femtosecond pulse and probed by another femtosecond pulse at a delayed time via either fluorescence (81) or ionization (56). The wave packet oscillates between the two turning points of the potential energy curve and its motion can be described by classical (82) and quantum (83) mechanics. The wave packet is a coherent superposition of adjacent vibrational eigenstates, and since each vibrational state has different energy, interferences among these states lead to time-dependent motion of the packet. The wave packet dephases gradually due to the anharmonicity of the potential. The time period for the wave packet to return to the original internuclear separation is determined by the energy differences

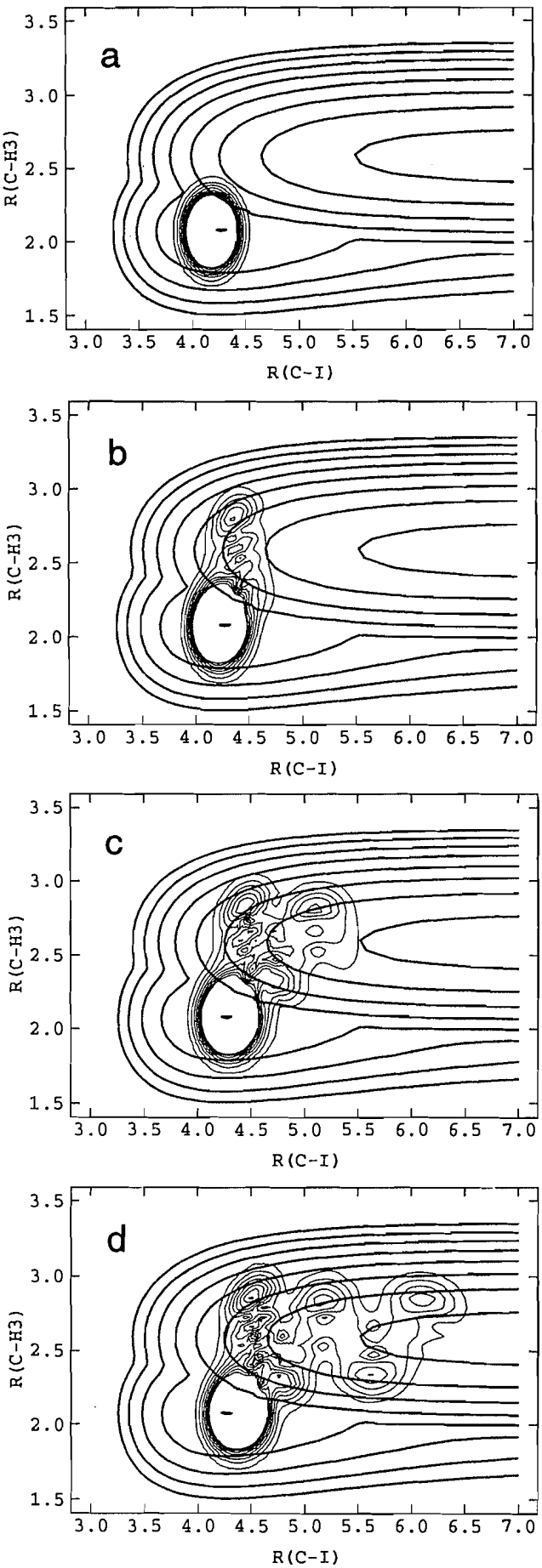

between adjacent levels. This type of coherence is universal to all processes involving elementary nuclear motions on various types of potentials (55).

Coherence can also exist between two states with different electronic characters provided they are appropriately coupled. In the case of methyl iodide, the band origin of the $7s[1]^2E_{3/2}$ state is only 240 cm^{-1} higher than the first ν_3 overtone on the $6p[4]^2E_{1/2}$ state. This can be seen from Fig. 6 where the vibrational levels are plotted with the potential energy surfaces of the $7s$ (dashed line) and $6p$ (dotted line) states. We have carried out calculations with two phase-locked ($\Delta\phi = 0$) femtosecond pulses tuned respectively to the two vibrational levels on the two Rydberg states. The transition dipole moment of the $7s[1]$ state was assumed to be a factor of two smaller than that of the $6p[4]$ state, in accordance with the experimental absorption spectrum (44, 46). Appropriate modifications of the Schrödinger equation were needed to include an extra state and two pump pulses. Although the two Rydberg states are not directly coupled, both of them are coupled with the dissociative state. Because of the energy difference between the two levels, interferences may arise and cause oscillations or quantum beats in the populations of the Rydberg states, which is reminiscence of the vibrational coherence in I_2. The calculated populations of both Rydberg levels are plotted with respect to time for both CH_3I (Fig. 8*a*) and CD_3I (Fig. 8*b*). It can be clearly seen that there is an oscillation with a frequency of approximately 140 fs throughout the decay of both CH_3I and CD_3I. Our calculated results give a reasonable account on the oscillatory feature observed in experiment although they are unable to offer a quantitative agreement, particularly at longer times. The disappearance of the oscillation in the later part of the dissociation is probably due to dephasing in a larger dimensional space which is not considered here.

One approximation we made in the calculations was to neglect the ionization pulse. Our rationale is based on the lack of knowledge of the ion state and the Franck–Condon nature of an ionization process. It should be pointed out that the oscillatory structure may also be attributed to the ionization process. Two ionization pathways exist during the probe process. One pathway is via the $6p[4]$ state while the other is via the $7s[1]$ state. Since the two Rydberg levels are prepared coherently by the pump pulse, the total ion signal is a square of the amplitude sum for the two pathways. Interferences will be important if the two pathways have comparable amplitudes. Furthermore, the energy difference of 240 cm^{-1} between the two Rydberg levels may survive the ionization and leads to the oscillations in the ion population in the first hundred femtoseconds (84, 85). The role played by the ionization in femtosecond pump-probe experiments certainly needs a more detailed analysis. It would be interesting to experimentally resolve the phase shift as the system executes the motion between the two states, in analogy with the experiment on iodine (86) and with the experiments on phase-shifted quantum beats for IVR studies (87).

FIG. 7. Snapshots of wave packet at 0 (*a*), 10 (*b*), 20 (*c*), and 30 (*d*) fs after a delta-function pulse excitation to the $6p[4]$ state. The heavy contours are the adiabatic potential energy surface formed by the Rydberg and repulsive states. The dissociation proceeds first along the C—H_3 vibrational coordinate and then to the C—I dissociation coordinate.

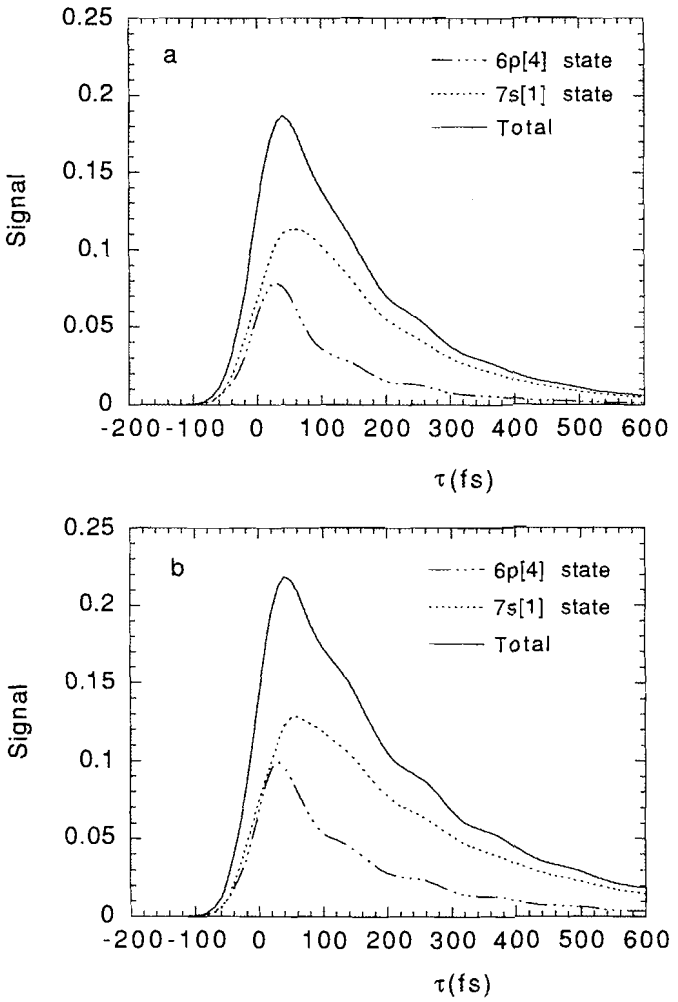

FIG. 8. Calculated transients for the broad bandwidth pulse excitation at 312 nm. Both the $6p[4]$ 3_0^1 and $7s[1]$ 0_0^0 Rydberg levels are excited coherently by the pulse. Oscillations with approximately 140 fs can be seen for both CH_3I (upper panel) and CD_3I (lower panel). The solid lines represent the total ion signal which is a sum of the signals from the two Rydberg states.

V. Conclusion

In summary, the femtosecond dynamics of Rydberg states, associated with the process of bond breakage in methyl iodide, involves more than one nuclear degree of freedom. This conclusion is based on experimental evidence of large isotope effects in the dissociation rate, which is indicative of the involvement of light atom tunneling in the dissociation. A two-dimensional model of the Rydberg predissociation dynamics of both methyl iodide and its deuterated isotope is advanced to account for the isotope effect, mode selectivity and coherence effects.

The two degrees of freedom involved in the model calculations are the C—I and C—H_3 coordinates. It is found that the predissociation of a methyl iodide Rydberg state involves non-adiabatic transitions to a dissociative state. Because the intersection between the Rydberg and dissociative states is perpendicular to the C—H_3 coordinate, the wave packet is forced to tunnel through the adiabatic barrier formed by the intersection and then dissociates. Since the predissociation involves tunneling of light atoms, a classical treatment of the dynamics becomes inappropriate. The calculations successfully reproduce the experimental observations and emphasize the importance of multidimensionality of the reaction pathway and the involvement of hydrogen (deuterium) atoms during the bond cleavage. We have also addressed the coherence effect induced by a broad bandwidth pump pulse. Although the model gives all the major features of the experimental results, it should be realized that the actual dynamics may involve many degrees of freedom. However, the present description may be sufficient for describing the elementary Rydberg state dynamics on the femtosecond scale.

For the future work, it would be advantageous to carry out *ab initio* calculations of the potential energy surfaces of the Rydberg and dissociative states of methyl iodide, which may help us to quantify the effect of the multidimensionality on the wave packet dynamics and on the non-adiabatic coupling. It would also be desirable to investigate the dynamics in the lower B and C bands in real-time in order to resolve some apparent controversies. Studies on this and other systems should be important to a broad class of Rydberg state dynamics, especially that the femtosecond time and mass resolutions make it possible to selectively isolate the elemental steps before long time events become operative.

Acknowledgments

This article is dedicated to John C. Polanyi, a colleague and friend, whose visionary and insightful work continues to inspire researchers in a number of areas covering science and humanity; it has certainly influenced the contribution reported here.

This work was funded by the donors of Petroleum Research Fund, administered by the American Chemical Society, by the National Science Foundation (CHE-9116501) to H.G., and by AFOSR to A.H.Z. Stimulating discussions with Marcos Dantus, Maurice Janssen and Volker Engel are gratefully acknowledged.

1. R.S. Mulliken. Phys. Rev. **47**, 413 (1935); R.S. Mulliken. Phys. Rev. **61**, 277 (1942); R.S. Mulliken and E. Teller, Phys. Rev. **61**, 283 (1942).
2. A. Gedanken and M.D. Rowe. Chem. Phys. Lett. **34**, 39 (1975).
3. J.L. Knee, L.R. Khundkar, and A.H. Zewail. J. Chem. Phys. **83**, 1996 (1985).
4. M.K. Dzvonik, S. Yang, and R. Bersohn. J. Chem. Phys. **61**, 4408 (1974).
5. S.J. Riley and K.R. Wilson. Faraday Discuss. Chem. Soc. **53**, 132 (1972).
6. T.F. Hunter and K.S. Krestjansson. Chem. Phys. Lett. **58**, 291 (1978).
7. P. Brewer, P. Das, G. Ondrey, and R. Bersohn. J. Chem. Phys. **79**, 720 (1983).
8. W.P. Hess, S.J. Kohler, H.K. Haugen, and S.R. Leone. J. Chem. Phys. **84**, 2143 (1986).
9. M.D. Barry and P.A. Gorry. Mol. Phys. **52**, 461 (1984).
10. G.N.A. van Veen, T. Baller, A.E. de Vries, and N.J.A. van Veen. Chem. Phys. **87**, 405 (1984).
11. S.L. Baughcum and S.R. Leone. J. Chem. Phys. **72**, 6531 (1980).
12. R.K. Sparks, K. Shobatake, L.R. Carlson, and Y.T. Lee. J. Chem. Phys. **75**, 3838 (1981).
13. H.W. Hermann and S.R. Leone. J. Chem. Phys. **76**, 4766 (1982).
14. R. Ogorzalek Loo, H.-P. Haerri, G.E. Hall, and P.L. Houston. J. Chem. Phys. **90**, 4222 (1989).
15. G.E. Hall, T.J. Sears, and J.M. Frye. J. Chem. Phys. **75**, 6234 (1989).
16. T. Suzuki, H. Kanamori, and E. Hirota. J. Chem. Phys. **94**, 6607 (1991).

17. J.F. Black and I. Powis. J. Chem. Phys. **89**, 3986 (1988); Chem. Phys. **125**, 375 (1988); I. Powis and J.F. Black. J. Phys. Chem. **93**, 2461 (1989),
18. D.W. Chandler, J.W. Thomas, Jr., M.H.M. Janssen, and D.H. Parker. Chem. Phys. Lett. **156**, 151 (1989); M.H.M. Janssen, D.H. Parker, G.O. Sitz, S. Stolte, and D.W. Chandler. J. Phys. Chem. **95**, 8007 (1991).
19. D. Imre, J.L. Kinsey, A. Sinha, and J. Krenos. J. Phys. Chem. **88**, 3956 (1984).
20. M.O. Hale, G.E. Galica, S.G. Glogover, and J.L. Kinsey. J. Phys. Chem. **90**, 4997 (1986).
21. K.Q. Lao, M.D. Person, P. Xayariboun, and L.J. Butler. J. Chem. Phys. **92**, 823 (1990).
22. G.E. Galica, B.R. Johnson, J.L. Kinsey, and M.O. Hale. J. Phys. Chem. **95**, 7994 (1991).
23. P.G. Wang and L.D. Ziegler. J. Phys. Chem. In press.
24. M. Tadjeddine, J.P. Flament, and C. Teichteil. Chem. Phys. **118**, 45 (1987).
25. Y. Amatatsu, K. Morokuma, and S. Yabushita. J. Chem. Phys. **94**, 4858 (1991).
26. M. Shapiro and R. Bersohn. J. Chem. Phys. **73**, 3810 (1980).
27. M. Shapiro. J. Phys. Chem. **90**, 3644 (1986).
28. H. Guo and G.C. Schatz. J. Chem. Phys. **93**, 393 (1990).
29. H. Guo, K.Q. Lao, G.C. Schatz, and A.D. Hammerich. J. Chem. Phys. **94**, 6562 (1991).
30. S.-Y. Lee and E.J. Heller. J. Chem. Phys. **76**, 3035 (1982).
31. S.K. Gray and M.S. Child. Mol. Phys. **51**, 189 (1984).
32. R.L. Sundberg, D. Imre, M.O. Hale, J.L. Kinsey, and R.D. Coalson. J. Phys. Chem. **90**, 5001 (1986).
33. H. Guo. Chem. Phys. Lett. **187**, 360 (1991); J. Chem. Phys. **96**, 6629 (1992).
34. G. Herzberg. Molecular spectra and molecular structure. Vol. 3. Krieger, Malabar. 1991.
35. M.B. Robin. Higher electronic states of polyatomic molecules. Vol. 1. Academic, New York. 1974.
36. S. Felps, P. Hochmann, P. Brint, and S.P. McGlynn. J. Mol. Spectros. **59**, 355 (1976).
37. D.H. Parker, R. Pandolfi, P.R. Stannard, and M.A. El-Sayed. Chem. Phys. Lett. **45**, 27 (1980).
38. S.P. Sapers and D.J. Donaldson. Chem. Phys. Lett. **173**, 257 (1990).
39. S.P. Sapers, V. Vaida, and R. Naaman. J. Chem. Phys. **88**, 3638 (1988).
40. D.J. Donaldson, V. Vaida, and R. Naaman. J. Chem. Phys. **87** 2522 (1987); J. Phys. Chem. **92**, 1204 (1988).
41. V. Vaida, D.J. Donaldson, S.P. Sapers, and R. Naaman. J. Chem. Soc. Faraday Trans. **86**, 2043 (1990).
42. V. Vaida, D.J. Donaldson, S.P. Sapers, R. Naaman, and M.S. Child. J. Phys. Chem. **93**, 513 (1989).
43. J.A. Syage. Chem. Phys. Lett. **212**, 124 (1993); J.A. Syage and J. Steadman. J. Phys. Chem. **94**, 7343 (1990).
44. A. Gedanken, M.B. Robin, and Y. Yafet. J. Chem. Phys. **76**, 4798 (1982).
45. K. Tsukiyama, B. Katz, and R. Bersohn. Chem. Phys. Lett. **124**, 309 (1986).
46. M.R. Dobber, W.J. Buma, and C.A. de Lange. J. Chem. Phys. **99**, 836 (1993).
47. K. Lao, M.D. Person, T. Chou, and L.J. Butler. J. Chem. Phys. **89**, 3463 (1988).
48. G.N.A. van Veen, T. Baller, and A.E. de Vries. Chem. Phys. **97**, 179 (1985).
49. L.D. Ziegler, Y.C. Chung, P.G. Wang, and Y.P. Zhang. J. Phys. Chem. **94**, 3394 (1990).
50. P.G. Wang, Y.P. Zhang, C.J. Ruggles, and L.D. Ziegler. J. Chem. Phys. **92**, 2806 (1990).
51. P.G. Wang and L.D. Ziegler. J. Chem. Phys. **95**, 288 (1991).
52. D.J. Campbell and L.D. Ziegler. J. Chem. Phys. **98**, 150 (1993).
53. D.J. Campbell and L.D. Ziegler. Chem. Phys. Lett. **201**, 159 (1993).
54. D.J. Donaldson, M.S. Child, and V. Vaida. J. Chem. Phys. **88**, 7410 (1988).
55. A.H. Zewail. Science, **242**, 1645 (1988); Faraday Discuss. Chem. Soc. **91**, 207 (1991).
56. M. Dantus, M.H.M. Janssen, and A.H. Zewail. Chem. Phys. Lett. **181**, 281 (1991).
57. M.H.M. Janssen, M. Dantus, H. Guo, and A.H. Zewail. Chem. Phys. Lett. **214**, 281 (1993).
58. H. Guo. Chem. Phys. Lett. **193**, 527 (1992).
59. E.E. Nikitin and M. Ya. Ovchinnikova. Chem. Phys. **138**, 45 (1989).
60. R.E. Continetti, B.A. Balko, and Y.T. Lee. J. Chem. Phys. **89**, 3383 (1988).
61. Faraday Discuss. Chem. Soc. **91** (1991); J. Phys. Chem. (1993); special issue on Femtochemistry.
62. R. Bersohn and A.H. Zewail. Ber. Bunsen-Ges. Phys. Chem. **92**, 373 (1988); R.B. Bernstein and R.B. Zewail. J. Chem. Phys. **90**, 829 (1989).
63. S.O. Williams and D.G. Imre. J. Phys. Chem. **92**, 6648 (1988); **92**, 6636 (1988).
64. V. Engel, H. Metiu, R. Almeida, R.A. Marcus, and A.H. Zewail. Chem. Phys. Lett. **152**, 1 (1988).
65. V. Engel and H. Metiu. J. Chem. Phys. **90**, 6116 (1989); **91**, 1596 (1989).
66. S.E. Choi and J.C. Light. J. Chem. Phys. **90**, 2593 (1989).
67. R. Heather and H. Metiu. Chem. Phys. Lett. **157**, 505 (1989).
68. H. Metiu and V. Engel. J. Chem. Phys. **93**, 5693 (1990).
69. V. Engel. Comp. Phys. Comm. **63**, 228 (1991).
70. S. Chapman and M.S. Child. J. Phys. Chem. **95**, 578 (1991).
71. M. Gruebele, G. Roberts, and A.H. Zewail. Phil. Trans. R. Soc. London, **A332**, 223 (1990).
72. R. Loudon. The quantum theory of light. Oxford University Press, Oxford. 1983.
73. V. Engel. Chem. Phys. Lett. **178**, 130 (1991).
74. M. Seel and W. Domcke. Chem. Phys. Lett. **151**, 59 (1991); J. Chem. Phys. **95**, 7806 (1991).
75. C. Leforestier, R. Bisseling, C. Cerjan, M.D. Feit, R. Friesner, A. Guldberg, A. Hammerich, G. Jolicard, W. Karrlein, H.D. Meyer, N. Lipkin, O. Roncero, and R. Kosloff. J. Comput. Phys. **94**, 59 (1991).
76. D. Kosloff and R. Kosloff. J. Comput. Phys. **52**, 35 (1983).
77. R. Heather and H. Metiu. J. Chem. Phys. **86**, 5009 (1987).
78. E.J. Heller. J. Chem. Phys. **68**, 2066 (1978).
79. R. Schinke. Photodissociation dynamics. Cambridge University Press, Cambridge. 1993.
80. S. Pedersen, L. Bañares, and A.H. Zewail. J. Chem. Phys. **97**, 8801 (1992).
81. R.M. Bowman, M. Dantus and A.H. Zewail. Chem. Phys. Lett. **161**, 297 (1989); M. Dantus, R.M. Bowman, and A.H. Zewail. Nature, **343**, 737 (1990).
82. R. Bernstein and A.H. Zewail. Chem. Phys. Lett. **170**, 321 (1990).
83. M. Gruebele, G. Roberts, M. Dantus, R.M. Bowman, and A.H. Zewail. Chem. Phys. Lett. **166**, 459 (1990); M. Gruebele and A.H. Zewail. J. Chem. Phys. **98**, 883 (1993).
84. T. Baumert, V. Engel, C. Meier, and G. Gerber. Chem. Phys. Lett. **200**, 488 (1993).
85. V. Engel, T. Baumert, C. Meier, and G. Gerber. Z. Phys. In press.
86. R.M. Bowman, M. Dantus, and A.H. Zewail. Chem. Phys. Lett. **174**, 546 (1990).
87. P. Felker and A.H. Zewail. Phys. Rev. Lett. **53**, 501 (1984); Adv. Chem. Phys. **70**, 265 (1988).